

Sol-gel entrapped visible light photocatalysts for selective conversions

Cite this: *RSC Adv.*, 2014, 4, 18341

Yanhui Zhang,^a Rosaria Ciriminna,^b Giovanni Palmisano,^c Yi-Jun Xu^{*a} and Mario Pagliaro^{*b}

A general method to heterogenize, stabilize and significantly enhance the activity of selective visible light photocatalysts for aerobic oxidation of glycerol is devised. The new method makes use of the sol-gel encapsulation of photocatalytic species in silica-based matrices to afford leach-proof catalysts capable to afford valued products at low cost with little or no waste generation. In particular, the photocatalytic selective conversion of glycerol is performed in water solvent under ambient conditions with molecular oxygen as oxidant and visible light as the driving energy source, thereby meeting all requirements for a green chemical process. Entrapment of the semiconductor-based photocatalyst inside the transparent porous silica matrix enhances substrate adsorption, thus improving its local concentration and favoring reaction with the photogenerated active species.

Received 5th February 2014
 Accepted 4th April 2014

DOI: 10.1039/c4ra01031k

www.rsc.org/advances

Semiconductor-based photocatalysis, especially using the semiconductor TiO₂, is generally a non-selective process suitable for degradation of organics, rather than for organic synthesis,¹ even though some progress towards more selective photosynthetic processes using modified titania has been achieved.² Further progress on semiconductor-based photocatalysis highlights that the appropriate choice of semiconductors (*e.g.*, tuning the structure, morphology and interface composition) and optimization of reaction parameters are able to promote the occurrence of photocatalytic organic synthesis with high selectivity.³

Recently, in the context of this progress, flower-like Bi₂WO₆ has been identified as a highly selective visible light photocatalyst toward aerobic selective oxidation of glycerol to dihydroxyacetone (DHA),⁴ using oxygen as oxidant in water at room temperature and atmospheric pressure. Besides meeting all requirements for a truly green chemical process, the method suggests the promising potential applications of semiconductor Bi₂WO₆-based photocatalysis in the field of biomass conversion to value-added fine chemicals under mild conditions.^{3,5}

Sol-gel silica is transparent to both visible and UV light radiation, and the sol-gel encapsulation is known to chemically and physically stabilize the entrapped species.⁶ Such a heterogenization strategy *via* sol-gel silica encapsulation provides a tunable control of microscopically confined environment surrounding the entrapped photoactive species, thereby tuning

the efficiency and selectivity of photocatalytic processes.^{7,8} Hence, in principle, entrapment of photocatalysts in transparent SiO₂ glasses might be desirable to stabilize, recover and reuse the entrapped photocatalyst. In particular, the entrapment within sol-gel silica can largely increase the surface area of catalyst, which would increase the adsorption capacity of catalyst toward reactant inside the sol-gel silica cages that consequently could contribute to the enhanced photoactivity. Yet, so far, only a few reports exist concerning sol-gel entrapped photocatalysts, even if a broad photochemistry of sol-gel doped glasses has been developed since the late 1980s.⁷

Two typical examples of entrapped photocatalysts are sodium decatungstate supported on sol-gel silica employed in the oxidation of glycerol under UV light irradiation,⁸ and silica-entrapped H₄SiW₁₂O₄₀ UV light photocatalyst used for the aerobic oxidation of various primary and secondary benzylic alcohols into the corresponding carbonyl compounds.⁹ However, to the best of our knowledge, no encapsulation of visible light photocatalyst has been previously reported for selective oxidation of glycerol. To develop highly photoactive visible-light-driven semiconductor-based photocatalyst is far more desirable than that of UV light photocatalyst, from a viewpoint of efficient and sustainable use of solar energy for practical applications. Herein, we report a simple and feasible method to directly transform flower-like Bi₂WO₆ into an entrapped sol-gel catalyst with enhanced photoactivity, retaining the high selectivity. The resulting silica-entrapped Bi₂WO₆ can be used as visible light photocatalyst for the aerobic selective conversion of glycerol to related products, such as dihydroxyacetone and glyceraldehyde, in water under ambient conditions. The as-obtained results are not trivial because reactivity, compared to the non-entrapped photocatalyst, in general is altered and can be greatly enhanced.

^aState Key Laboratory of Photocatalysis on Energy and Environment, College of Chemistry and Chemical Engineering, Fuzhou University, Fuzhou 350002, P.R. China. E-mail: yjxu@fzu.edu.cn

^bIstituto per lo Studio dei Materiali Nanostrutturati, CNR, via U. La Malfa 153, 90146 Palermo, Italy. E-mail: mario.pagliaro@cnr.it

^cDipartimento di Fisica e Chimica, Università degli Studi di Palermo, viale delle Scienze, 90128 Palermo, Italy

Data in Table 1 show that the two silica-entrapped Bi_2WO_6 catalysts are highly active, despite with remarkable differences in selectivity. Results are indeed impressive because now 8 mg of entrapped catalyst are enough to catalyze the reaction at noticeable extent. We are dealing indeed with 8 mg of silica-entrapped catalysts whose content of visible-light-photoactive bismuth tungstate (Bi_2WO_6) varies between 5 and 10% in weight. Hence, even using 1/20 and 1/10 the amount of 8 mg of non-entrapped Bi_2WO_6 used in previous work,⁴ the conversion of glycerol over silica-entrapped $\text{Bi}_2\text{WO}_6(1)$ and $\text{Bi}_2\text{WO}_6(2)$ proceeds up to 41% and 58%, respectively, under visible light irradiation for 10 h.

A direct comparison of glycerol conversion over 8 mg of silica-entrapped $\text{Bi}_2\text{WO}_6(2)$ (10% w/w catalyst loading, the photoactive Bi_2WO_6 is 0.8 mg) and 0.8 mg of non-entrapped Bi_2WO_6 [$\text{Bi}_2\text{WO}_6(2)$] under visible light irradiation of 4 h clearly shows that the photoactivity for glycerol conversion over silica-entrapped $\text{Bi}_2\text{WO}_6(2)$ is indeed greatly enhanced. That is, under visible light irradiation for 4 h using one tenth the amount of non-entrapped Bi_2WO_6 , the conversion of glycerol reaches 29%, which is more than 3 times higher than that over non-entrapped Bi_2WO_6 .⁴

In addition, it is worth noting that the catalyst of higher loading $\text{Bi}_2\text{WO}_6(2)$ retains the original high selectivity to DHA of the non-entrapped Bi_2WO_6 photocatalyst.⁴ However, this is not the case for the silica-entrapped catalyst $\text{Bi}_2\text{WO}_6(1)$ with lower loading of Bi_2WO_6 . This means that the loading amount of bismuth wolframate entrapped within silica alters not only the photoactivity but also the selectivity of the entrapped catalyst (see below for our tentative explanation of this finding).

The XRD patterns in Fig. 1 show that crystalline, well characterized Bi_2WO_6 crystals are encapsulated within the silica xerogels in both cases of 5% w/w and 10% w/w catalyst loading, suggesting that the silica encapsulation does not destroy the crystalline phase structure of Bi_2WO_6 (JCPDS no. 73-1126).

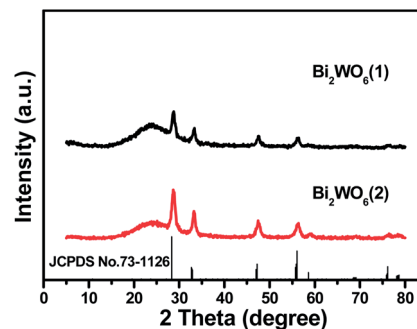


Fig. 1 XRD patterns of the samples of silica-entrapped Bi_2WO_6 .

The SEM pictures of the silica-entrapped Bi_2WO_6 samples, as shown in Fig. 2, suggest that, due to the encapsulation of silica, the flower-like structure of non-entrapped Bi_2WO_6 cannot be directly observed. In its place, matrix particles made of amorphous silica are clearly observed. The ground granules obtained from grinding a sol-gel monolith, furthermore, have the irregular shape, angular geometry and multiple cracks, which are typical of silica xerogel particles.¹⁰

Fig. 3 shows the TEM images of sol-gel entrapped $\text{Bi}_2\text{WO}_6(2)$ sample. It can be seen that, during the entrapping process, the flower-like superstructure of original Bi_2WO_6 is destroyed. However, the basic unit comprising superstructure of flower-like Bi_2WO_6 is still retained.⁴ Also, the silica encapsulating shell for sol-gel entrapped $\text{Bi}_2\text{WO}_6(2)$ sample can be clearly distinguished. The bottom image shows the outcome of electron diffraction of regions, from which it is seen that the crystalline structure of Bi_2WO_6 is clearly retained upon the sol-gel encapsulation, where the sol-gel silica shows its amorphous nature.

The optical properties, as reflected by the UV-visible diffuse reflectance spectra (DRS) of the samples of two entrapped catalysts in Fig. 4, clearly show that the materials can be band-

Table 1 Photocatalytic selective oxidation of glycerol over non-entrapped Bi_2WO_6 and over silica-entrapped Bi_2WO_6 catalyst under the irradiation of visible light in water^a

Photocatalyst	Time (h)	Conversion (%) glycerol	Selectivity (%)		
			Dihydroxyacetone	Glyceraldehyde	Others
$\text{Bi}_2\text{WO}_6(1)$	2	11	63	28	9
	4	20	62	27	11
	6	28	58	25	17
	8	35	55	24	21
	10	41	53	24	23
Non-entrapped $\text{Bi}_2\text{WO}_6(1)$	2	3	95	5	0
	4	5	93	7	0
$\text{Bi}_2\text{WO}_6(2)$	2	16	97	3	0
	4	29	95	5	0
	6	40	94	5	1
	8	50	92	6	2
	10	58	91	6	3
	4	9	93	7	0

^a Reaction conditions: 0.1 mmol glycerol, 1.5 mL H_2O , $T = 25^\circ\text{C}$, visible light $>420\text{ nm}$. For purposeful comparison, the amount of non-entrapped Bi_2WO_6 used for photocatalytic oxidation of glycerol is the same as that of Bi_2WO_6 in silica-entrapped Bi_2WO_6 namely 0.8 mg for $\text{Bi}_2\text{WO}_6(2)$ and 0.4 mg for $\text{Bi}_2\text{WO}_6(1)$.

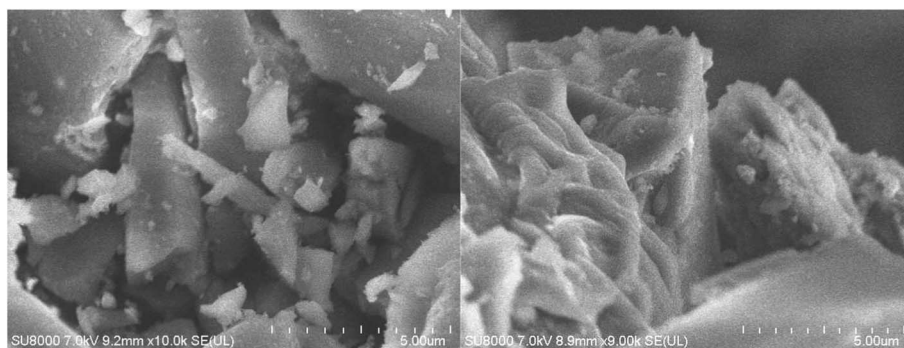


Fig. 2 Typical SEM pictures of the samples of silica-entrapped $\text{Bi}_2\text{WO}_6(1)$ (left) and $\text{Bi}_2\text{WO}_6(2)$ (right).

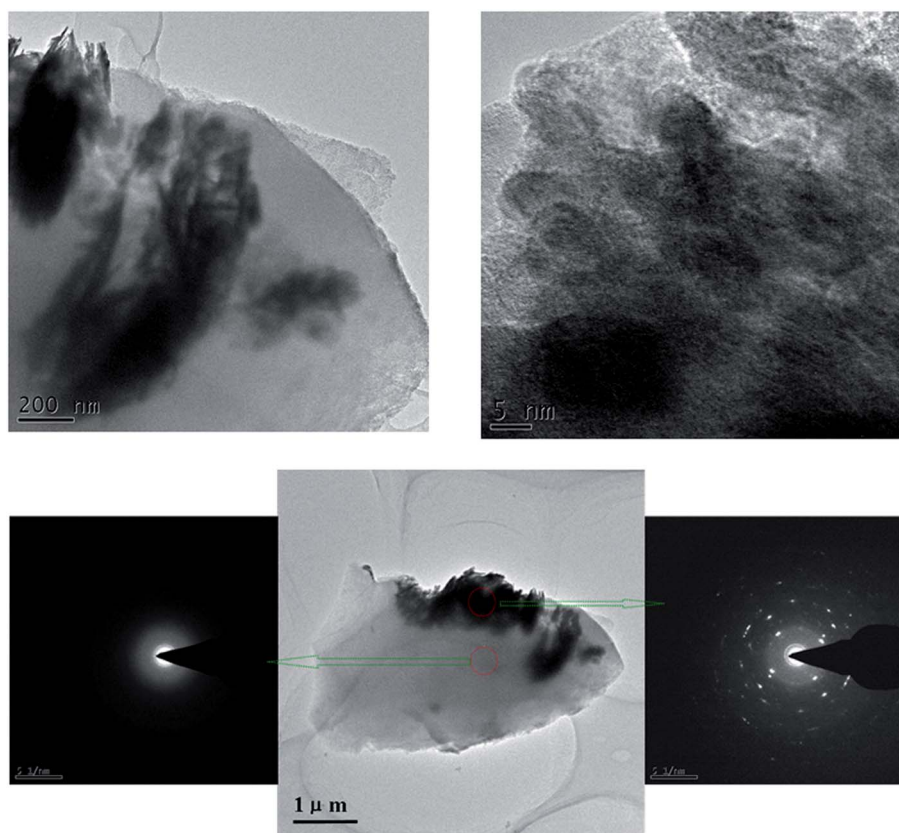


Fig. 3 Top: TEM pictures of the samples of silica-entrapped $\text{Bi}_2\text{WO}_6(2)$. Bottom: images showing the outcome of electron diffraction of different sample regions.

gap-photoexcited by visible light irradiation, but at different extent because of their difference in optical absorption. As expected, due to the higher loading of photoactive Bi_2WO_6 for silica-entrapped $\text{Bi}_2\text{WO}_6(2)$, the latter catalyst sample has stronger light absorption intensity than $\text{Bi}_2\text{WO}_6(1)$ in both the UV and visible light regions.

The photoluminescence (PL) spectra are often employed to study surface processes involving the electron–hole fate of the semiconductor. Following the electron–hole pairs recombination after a photocatalyst is irradiated, photons are emitted, which results in PL signal. As shown in Fig. 5, the PL intensity obtained over silica-entrapped $\text{Bi}_2\text{WO}_6(2)$ is clearly weaker than

that of $\text{Bi}_2\text{WO}_6(1)$, thus suggesting the longer lifetime of photogenerated charge carriers. Thus, the presence of different amounts of SiO_2 affects the PL intensity for SiO_2 -entrapped Bi_2WO_6 , thereby contributing to the photoactivity difference between two different samples, *i.e.*, silica-entrapped $\text{Bi}_2\text{WO}_6(1)$ and silica-entrapped $\text{Bi}_2\text{WO}_6(2)$.

Notably, the photoluminescence (PL) spectra in Fig. 5 clearly show that: (i) the PL intensity of silica-entrapped Bi_2WO_6 is much lower than that of non-entrapped Bi_2WO_6 , indicating that the sol-gel silica encapsulation contributes to the improved separation of photogenerated electron–hole pairs of Bi_2WO_6 under visible light irradiation; (ii) the confinement of Bi_2WO_6

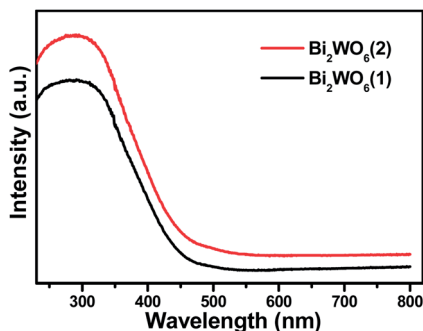


Fig. 4 The UV-visible diffuse reflectance spectra (DRS) of the samples of silica-entrapped Bi_2WO_6 .

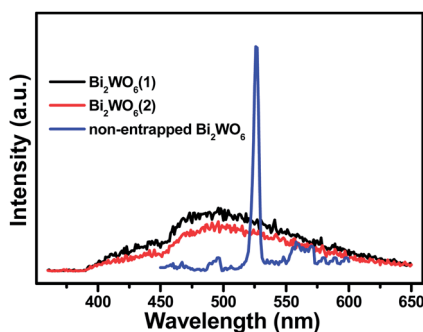


Fig. 5 The photoluminescence (PL) spectra of the samples of silica-entrapped Bi_2WO_6 and non-entrapped Bi_2WO_6 with an excitation wavelength of 340 nm.

nanocrystals resulting from sol-gel silica encapsulation leads to the significantly different PL emission profiles, suggesting that the synergistic interaction between silica and Bi_2WO_6 influences the spatial transfer kinetics (in addition to improving the lifetime of photogenerated electron-hole pairs).

Together, these factors already mentioned above may account for the difference in both photoactivity and selectivity in the aerobic oxidation of glycerol over silica-entrapped Bi_2WO_6 with different amounts of silica and non-entrapped Bi_2WO_6 . Under visible light irradiation, holes and electrons generated inside the Bi_2WO_6 crystalline phase diffuse to the surface of the inner porosity of the silica cages, where they can react with the incoming organic molecules. In brief, the combined effects of semiconductor confinement in the silica cages^{6,8-10} and synergistic interaction of Bi_2WO_6 with the SiO_2 cage play a crucial role in affecting the selectivity and activity for oxidation of glycerol.

Table 2 Textural properties of non-entrapped Bi_2WO_6 , silica-entrapped $\text{Bi}_2\text{WO}_6(1)$ and $\text{Bi}_2\text{WO}_6(2)$ based on the N_2 adsorption-desorption isotherms

Sample	S_{BET} ($\text{m}^2 \text{g}^{-1}$)	Total pore volume ($\text{cm}^3 \text{g}^{-1}$)	Average pore size (nm)
Non-entrapped Bi_2WO_6	31	0.16	5 and 42
$\text{Bi}_2\text{WO}_6(1)$	964	0.56	2
$\text{Bi}_2\text{WO}_6(2)$	517	0.30	2

Table 2 shows the data based on the analysis of N_2 adsorption-desorption isotherms of silica-entrapped catalyst $\text{Bi}_2\text{WO}_6(1)$ and $\text{Bi}_2\text{WO}_6(2)$, and non-entrapped Bi_2WO_6 . $\text{Bi}_2\text{WO}_6(1)$ has huge specific surface area (*ca.* $964 \text{ m}^2 \text{g}^{-1}$) along with significant specific pore volume (*ca.* $0.56 \text{ cm}^3 \text{g}^{-1}$). For the higher loading sample, *i.e.*, silica-entrapped $\text{Bi}_2\text{WO}_6(2)$, the surface area is reduced to *ca.* $517 \text{ m}^2 \text{g}^{-1}$ and the pore volume is *ca.* $0.30 \text{ cm}^3 \text{g}^{-1}$. Comparison to non-entrapped Bi_2WO_6 , with low surface area of *ca.* $31 \text{ m}^2 \text{g}^{-1}$ and pore volume of *ca.* $0.16 \text{ cm}^3 \text{g}^{-1}$, clearly shows that the sol-gel entrapment significantly increases the surface area of the samples.

Adsorption experiments in the dark shown in Fig. 6 indeed confirm that samples of silica-entrapped Bi_2WO_6 have enhanced adsorption capacity toward glycerol as compared to the non-entrapped Bi_2WO_6 .⁴ Such an enhanced adsorption capacity reminds one that glycerol can be easily adsorbed and concentrated at the surface of the silica sol-gel cages, with their numerous silanol groups. The very same cages entrap the photocatalytic crystallites and act as chemical sponges that adsorb and concentrate reactants at their surface.¹¹ The adsorbed glycerol molecules further react at the surface of entrapped Bi_2WO_6 to be oxidized by the positive holes to form the corresponding intermediate, which further reacts with oxygen or activated oxygen to produce DHA and other related products.⁴

However, it should be noted that the surface area is not the only factor that determines the overall photoactivity and selectivity in the photocatalytic oxidation of glycerol. The sample of silica-entrapped $\text{Bi}_2\text{WO}_6(1)$ has much higher surface area and pore volume than silica-entrapped catalyst $\text{Bi}_2\text{WO}_6(2)$. But the photoactivity of $\text{Bi}_2\text{WO}_6(1)$ is lower than $\text{Bi}_2\text{WO}_6(2)$. This can be attributed to the higher amount loading of photoactive Bi_2WO_6 photoactive species in the silica-entrapped $\text{Bi}_2\text{WO}_6(2)$, which has a higher visible light absorption capacity and longer lifetime of photogenerated electron-hole pairs, that are the crucial factors determining the overall efficiency of photocatalytic process.

In addition, as discussed above, with the variation of loading amount of photoactive Bi_2WO_6 ingredients in the silica matrix,

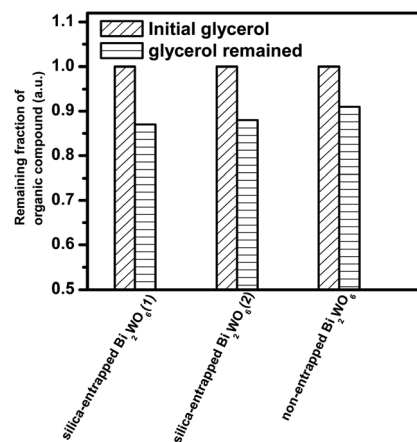


Fig. 6 Remaining fraction of glycerol after the adsorption-desorption equilibrium in the dark over silica-entrapped $\text{Bi}_2\text{WO}_6(1)$, silica-entrapped $\text{Bi}_2\text{WO}_6(2)$, and non-entrapped flower-like Bi_2WO_6 .

the selectivity is also affected, suggesting that a synergy interaction between the silica matrix and photoactive Bi_2WO_6 exists in the silica-entrapped Bi_2WO_6 photocatalysts. Silanols at the surface of the sol-gel silica cages favour adsorption of glycerol, enhancing its local concentration and thus easing its reaction with photogenerated active charge carriers including activated molecular oxygen at the cage surface. However, when an insufficient amount of photoactive Bi_2WO_6 is encapsulated, the glycerol molecules are preferentially adsorbed through their more reactive and less hindered primary hydroxyl groups, thereby affording considerable formation of glyceraldehyde (Table 1). In contrast, when a sufficient amount of encapsulated Bi_2WO_6 is available for reactivity at the sol-gel cages, glycerol is again preferentially oxidised at the secondary OH group, showing the remarkable effect of both the encapsulating silica matrix and loading of photoactive Bi_2WO_6 species on selectivity toward selective photocatalytic oxidation of glycerol. This effect, we argue, is due to the templating action of the dopant species during the sol-gel hydrolytic polycondensation, in which the dopant species dictate the size and the shape of the encapsulating silica cage in the final xerogel.¹²

In conclusion, we have shown that the sol-gel encapsulation of flower-like Bi_2WO_6 microparticles in SiO_2 xerogels leads to the formation of excellent visible-light-driven photocatalytic materials with great potential to act as solar energy transfer materials. The transparent, stabilizing and high surface area of the encapsulated silica matrix allows light penetration, promoting the efficiency of the photogenerated electron-hole separation and enhancing adsorption capacity toward glycerol. As a result, the photoactivity in the aerobic selective oxidation of glycerol under visible light irradiation over silica-entrapped Bi_2WO_6 is greatly enhanced. The synergy between the silica matrix and photoactive entrapped Bi_2WO_6 allows the tunable control of both activity and selectivity for photocatalytic oxidation of glycerol under visible light irradiation.

Glycerol demonstrated herein is just one example of a biomass-derived chemical suitable for chemical upgrade.^{13,14} Many other biomass molecules could react, including organic molecules that are not water soluble, and be readily converted to value-added fine chemicals using this SiO_2 xerogels trapped semiconductor composite photocatalyst. Further work is in progress to expand the scope of this simple and feasible method.

Experimental section

The catalyst hydrothermal sol-gel synthesis starts from flower-like Bi_2WO_6 prepared following the published procedure.⁴ In detail, the simple hydrothermal synthesis starts with sonication of $\text{Bi}(\text{NO}_3)_3 \cdot 5\text{H}_2\text{O}$ (0.98 g) in 40 mL of 0.3 M HNO_3 aqueous solution. Then, 20 mL of 0.05 M $\text{Na}_2\text{WO}_4 \cdot 2\text{H}_2\text{O}$ solution was added with vigorous stirring and a white precipitate was formed. Subsequently, a NaOH solution (20 mL, 0.2 M) was added under stirring, mixing the resulting solution for 24 h. This mixture was then transferred to a 100 mL Parr autoclave and maintained at 160 °C for 8 h. The resulting sample was recovered by filtration, washed by water, and fully dried at 60 °C in oven to get the final flower-like Bi_2WO_6 samples.

Two sol-gel entrapped catalysts were prepared using TEOS (tetraethylorthosilicate, $\text{Si}(\text{OCH}_3)_4$) as silica precursor. In one typical preparation, 150 mg of flower-like Bi_2WO_6 was suspended in 1 mL H_2O and the suspension was kept stirring for 30 minutes. The required amount of TEOS (0.025 mol for the 10 wt% catalyst and 0.05 mol for the 5 wt% catalyst) was added to an aqueous solution of HCl 0.05 N and stirred for 30 minutes. After this pre-hydrolysis step, the suspension of Bi_2WO_6 was added and the resulting mixture was kept under mechanical stirring for 30 minutes, after which an aliquot of NaOH 1 N (0.1 mL for 10 wt% and 0.18 mL for 5 wt%) was added. Gelification rapidly occurred.

The resulting alcogel was left in a closed vessel for 24 h after which the vessel was opened and left for 3 days at room temperature and pressure (ambient conditions). The doped silica glass monolith thereby obtained was mildly powdered in a mortar and used as such. The sol-gel encapsulated catalyst sample $\text{Bi}_2\text{WO}_6(1)$ has a 5% w/w catalyst loading, and $\text{Bi}_2\text{WO}_6(2)$ has a 10% w/w catalyst loading. To check the materials synthesis reproducibility, similar catalysts (not shown) were prepared also in China using the same methodology. Almost identical results were obtained both for the materials and their synthetic application, confirming full reproducibility of both sol-gel materials synthesis and hydrothermal synthesis of flower-like Bi_2WO_6 .

The morphology information was determined by a field-emission scanning electron microscope (FESEM, FEI Nova NANOSEM 230). Transmission electron microscopy (TEM) images were collected using a JEOL model JEM 2010 EX microscope at an accelerating voltage of 200 kV. The crystalline structure of the catalysts was determined by powder X-ray diffraction (XRD), using Ni-filtered $\text{Cu K}\alpha$ radiation in the 2θ range from 5° to 80° with a scan rate of 0.08° per second. The optical properties of the catalysts were analyzed by UV-vis diffuse reflectance spectroscopy (DRS) using a Cary-500 spectrophotometer over a wavelength range of 230–800 nm, during which BaSO_4 was employed as the internal reflectance standard. Nitrogen adsorption-desorption isotherms and the Brunauer-Emmett-Teller (BET) surface area were collected at 77 K using Micromeritics ASAP 2010 equipment. The photoluminescence (PL) spectra were measured on an Edinburgh FL/FS900 spectrophotometer. For the PL analysis of solid samples of Bi_2WO_6 , the excitation wavelength is 340 nm. The PL spectra are often employed to study surface processes involving the electron-hole fate of semiconductor. With the electron-hole pairs recombination after a semiconductor photocatalyst is irradiated, photons are emitted, thus resulting in PL. Thus, the PL analysis reflects the fate of electron-hole pairs photogenerated from semiconductor Bi_2WO_6 encapsulated into the sol-gel silica matrix.

The aerobic oxidation of glycerol in water was carried out in a 10 mL Pyrex glass bottle under the irradiation of visible light using a 300 W Xe arc lamp with a UV cutoff filter ($\lambda > 420$ nm). In a typical process, a mixture of 8 mg solid catalyst and 0.1 mmol of glycerol were added to 1.5 mL water. The mixture, saturated with pure molecular oxygen from a gas cylinder, was transferred into a 10 mL Pyrex glass bottle and stirred for 10 min. After the reaction, the mixture was centrifuged at 12 000 rpm for 20 minutes to separate and remove the catalyst particles. The

remaining solution was analyzed with a Shimadzu Liquid Chromatograph (DGU-20A3, equipped with a 512 Diode Array Detector and a C18 analysis column).

Acknowledgements

This article is dedicated to University of Palermo's Professor Giuseppe Aiello for his excellent teaching of physics at chemistry students spanning his lifetime career. We thank PhD student Piera Demma Carà for preparing preliminary catalytic samples. The support by the NSFC (21173045, 20903023), the Award Program for Minjiang Scholar Professorship, the NSF of Fujian Province for Distinguished Young Investigator Grant (2012J06003), and Program for Returned High-Level Overseas Chinese Scholars of Fujian Province is gratefully acknowledged.

References

- 1 V. Augugliaro, V. Loddo, M. Pagliaro, G. Palmisano and L. Palmisano, *Clean by Light Irradiation*, RSC Publishing, Cambridge, UK, 2010.
- 2 (a) G. Palmisano, V. Augugliaro, M. Pagliaro and L. Palmisano, *Chem. Commun.*, 2007, 3425; (b) N. Zhang, Y. Zhang and Y.-J. Xu, *Nanoscale*, 2012, 4, 5792; (c) N. Zhang, S. Liu and Y.-J. Xu, *Nanoscale*, 2012, 4, 2227.
- 3 (a) M.-Q. Yang and Y.-J. Xu, *Phys. Chem. Chem. Phys.*, 2013, 15, 19102; (b) N. Zhang, M.-Q. Yang, Z.-R. Tang and Y.-J. Xu, *ACS Nano*, 2014, 8, 623; (c) M. Cherevatskaya, S. Fuldner, C. Harlander, M. Neumann, S. Kummel, S. Dankesreiter, A. Pfitzner, K. Zeitler and B. Konig, *Angew. Chem., Int. Ed.*, 2012, 51, 4062; (d) Y. Zhang, N. Zhang, Z.-R. Tang and Y.-J. Xu, *ACS Nano*, 2012, 6, 9777; (e) B. Weng, S. Liu, Z.-R. Tang and Y.-J. Xu, *RSC Adv.*, 2014, 4, 12865.
- 4 Y. Zhang, N. Zhang, Z.-R. Tang and Y.-J. Xu, *Chem. Sci.*, 2013, 4, 1820.
- 5 C.-H. Zhou, X. Xia, C.-X. Lin, D.-S. Tong and J. Beltramini, *Chem. Soc. Rev.*, 2011, 40, 5588.
- 6 M. Pagliaro, R. Ciriminna and G. Palmisano, *Chem. Soc. Rev.*, 2007, 36, 932.
- 7 (a) A. Slama-Schwok, D. Avnir and M. Ottolenghi, *Photochem. Photobiol.*, 1991, 54, 525; (b) B. Dunn and J. Zink, *J. Mater. Chem.*, 1991, 1, 903.
- 8 A. Molinari, A. Maldotti, A. Bratovcic and G. Magnacca, *Catal. Today*, 2013, 206, 46.
- 9 S. Farhadi, Z. Babazadeh and M. Maleki, *Acta Chim. Slov.*, 2006, 53, 72.
- 10 R. Ciriminna, A. Fidalgo, F. Béland, V. Pandarus, L. M. Ilharco and M. Pagliaro, *Chem. Rev.*, 2013, 113, 6592.
- 11 D. Avnir, *Acc. Chem. Res.*, 1995, 28, 328.
- 12 This effect has been reported for several encapsulated species. For example, flavor molecules: (a) S. R. Veith, M. Perren and S. E. Pratsinis, *J. Colloid Interface Sci.*, 2005, 283, 495; chiral species: (b) S. Fireman Shores, S. Marx and D. Avnir, *Adv. Mater.*, 2007, 19, 2145; and catalytic ion pairs: (c) R. Ciriminna and M. Pagliaro, *Chem. Eur. J.*, 2003, 9, 5067.
- 13 M. Pagliaro, R. Ciriminna, H. Kimura, M. Rossi and C. Della Pina, *Angew. Chem., Int. Ed.*, 2007, 46, 4434.
- 14 A. Corma, S. Iborra and A. Velty, *Chem. Rev.*, 2007, 107, 2411.